

## Activation energy for the loss of substitutional carbon in $\text{Si}_{0.984}\text{C}_{0.016}$ grown by solid phase epitaxy

Yong Jeong Kim,\*<sup>1</sup> Tae-Joon Kim,<sup>1</sup> Byungwoo Park,<sup>1</sup> and Jong Han Song<sup>2</sup>

<sup>1</sup>School of Materials Science and Engineering, Seoul National University, Seoul, Korea

<sup>2</sup>Korea Institute of Science and Technology, Seoul, Korea

(Received May 4, 2000)

**Abstract** – We studied the synthesis of  $\text{Si}_{1-x}\text{C}_x$  ( $x = 0.016$ ) epitaxial layer using ion implantation and solid phase epitaxy (SPE). The activation energy  $E_a$  was obtained for the loss of substitutional carbon using fourier transform-infrared spectroscopy (FTIR) and high-resolution x-ray diffraction (HR-XRD). In FTIR analysis, the integrated peak intensity was used to quantify the loss of carbon atoms from substitutional to interstitial sites during annealing. The substitutional carbon contents in  $\text{Si}_{0.984}\text{C}_{0.016}$  were also measured using HR-XRD. By dynamic simulations of x-ray rocking curves, the fraction of substitutional carbon was obtained. The effects of annealing temperature and time were also studied by comparing vacuum furnace annealing with rapid thermal annealing (RTA).

**Keywords** – SPE,  $\text{Si}_{1-x}\text{C}_x$ , FTIR, HR-XRD, substitutional carbon, RTA

### I. Introduction

Group IV heteroepitaxial materials grown on Si substrates have been investigated as bandgap engineering materials. In particular,  $\text{Si}_{1-x}\text{Ge}_x$  epitaxial material has been extensively studied because of significant potential for the fabrication of high speed devices and optoelectronic device applications [1, 2]. SiGe-based heterojunction bipolar transistors (HBTs) have high current gain and superior speed compared with equivalent Si device because the heterojunction between SiGe base and Si emitter can improve the emitter injection efficiency [1, 3-5]. SiGe channel field-effect transistor (FET) shows higher hole mobility and transconductance compared with equivalent Si device [6]. However,  $\text{Si}_{1-x}\text{Ge}_x$  exhibits some severe limitations for device applications [3-5, 7-9]. The first is critical thickness for thermal stability against misfit-dislocation formation due to lattice mismatch. Second, main bandoffset appears at valence band. Hence,  $\text{Si}_{1-x}\text{Ge}_x$  is better suited as a hole channel than as an electron channel. Third,  $\text{Si}_{1-x}\text{Ge}_x$  has some difficulty in controlling dopant diffusion.

Recently, it was shown that the incorporation of carbon into substitutional sites could overcome some of the limitations [3, 8-11]. Ion implantation and

solid phase epitaxy (SPE) have been used successfully to incorporate carbon into substitutional sites. However, due to the low solubility of carbon in Si,  $\beta$ -SiC is formed during epitaxial regrowth [7-9, 12]. Also, because carbon retards the SPE rates, higher regrowth temperature may be needed [13-16]. Despite these conflicting problems, Strane *et al.* [14-16] have shown that carbon can be successfully incorporated into substitutional sites using ion implantation followed by SPE.

In this paper, we discuss the formation of  $\text{Si}_{0.984}\text{C}_{0.016}$  epitaxial layers using SPE. The activation energy for the loss of substitutional carbon is obtained from fourier-transform infrared spectroscopy (FTIR) and high-resolution x-ray diffraction (HR-XRD). The effects of annealing temperature and time are also studied by comparing vacuum furnace annealing and rapid thermal annealing (RTA).

### II. Experimental Details

The  $\text{Si}_{0.984}\text{C}_{0.016}$  layers were epitaxially grown on  $\sim 6 \Omega\text{cm}$  Si (100) substrates. The thickness of wafer was approximately 500  $\mu\text{m}$ . Double-side polished wafers were used to reduce the background signal and noise during FTIR measurements. Ion implanta-

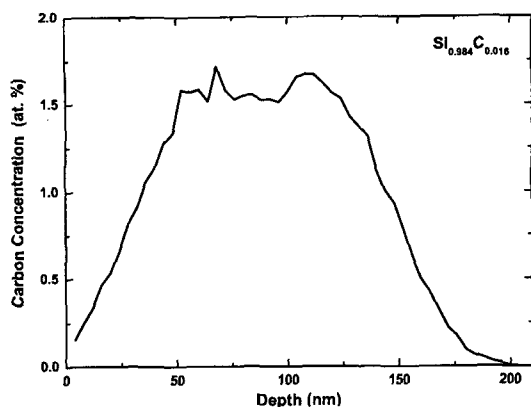


Fig. 1. Carbon depth profile obtained by TRIM simulation.

tions were performed at room temperature at KIST-National Electrostatics Corp. Energies and doses of ions were determined from TRIM simulation. Before carbon implantation, the Si surface was preamorphized by Si with 50 and 100 keV at  $2 \times 10^{15}$  and  $8 \times 10^{15}$   $\text{Si}^-/\text{cm}^2$ , respectively. Carbon implantation energies and doses, designed to get uniform carbon profile, were 15 and 29 keV at  $2 \times 10^{15}$  and  $7.2 \times 10^{15}$   $\text{C}^-/\text{cm}^2$ , respectively. According to TRIM simulation, carbon profile is relatively flat from approximately 50 nm to 135 nm with a carbon concentration of approximately 1.6 at. %, as shown in Fig. 1.

Annealing was performed in a fused silica tube

furnace under  $1 \times 10^{-6}$  Torr or RTA under constant  $\text{N}_2$  flow. The  $\text{Si}^-$  and  $\text{C}^-$  implanted samples were regrown epitaxially after sequential two-step annealing, at  $500^\circ\text{C}$  for 30 min plus at  $700^\circ\text{C}$  for 30 min. After regrowth, samples were annealed at  $800^\circ\text{C}$ ,  $850^\circ\text{C}$ , and  $900^\circ\text{C}$ , respectively. RTA was performed at  $950^\circ\text{C}$  and  $1000^\circ\text{C}$  for 10 sec or 30 sec.

To minimize absorption due to ambient gases during FTIR measurements, these were performed in vacuum ( $<0.1$  Torr), and all measurements were performed at room temperature (by using Bomem DA 8.16). In order to obtain carbon content from FTIR data, subtraction of signal from a reference sample without ion implantation was performed. To minimize background error due to surface oxidation, each reference sample was annealed under the same condition. HR-XRD measurements were performed by using Bede Scientific Instruments. In order to characterize substitutional carbon contents, rocking curve data were fitted by dynamic simulations.

### III. Results and Discussion

FTIR absorption spectra of  $\text{Si}_{0.984}\text{C}_{0.016}$  layers annealed at  $850^\circ\text{C}$  or  $900^\circ\text{C}$  for different time is shown in Fig. 2. Substitutional carbon in Si has a local vibration mode at  $607\text{ cm}^{-1}$  and  $\beta\text{-SiC}$  has a phonon absorption mode at  $810\text{ cm}^{-1}$  [15]. As shown

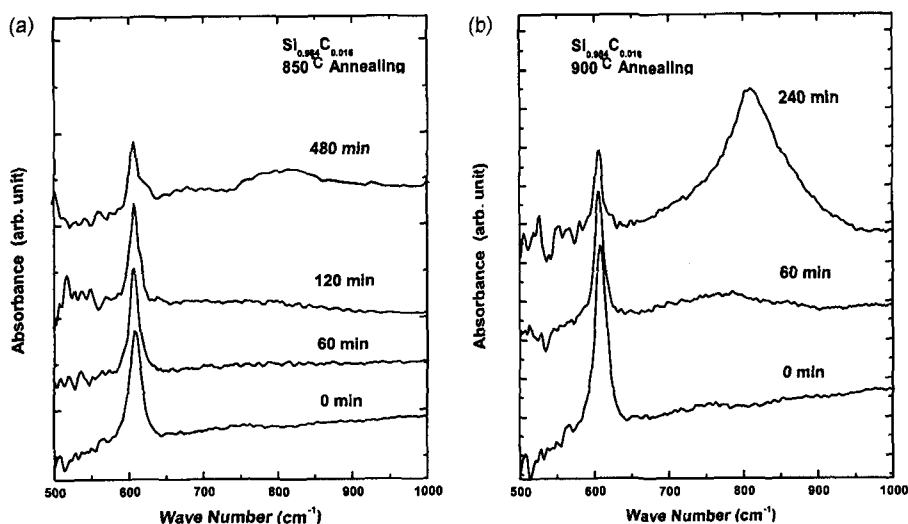
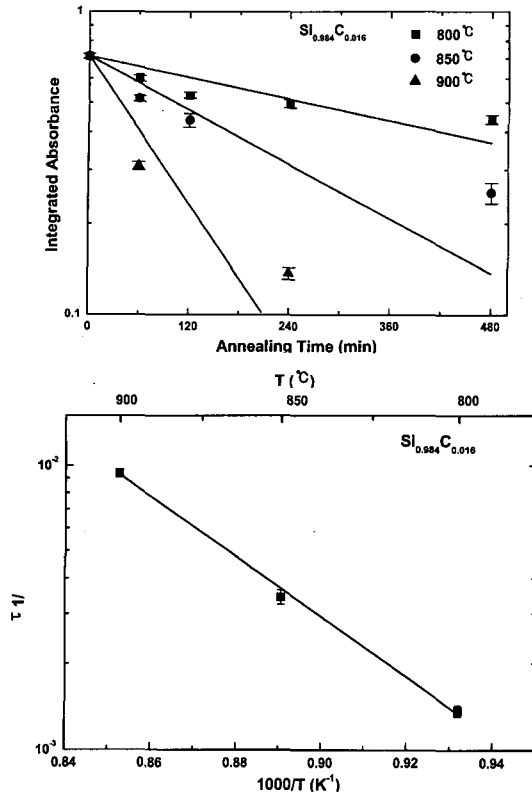


Fig. 2. (a) FTIR absorption spectra for  $\text{Si}_{0.984}\text{C}_{0.016}$  alloy layer after annealing at  $850^\circ\text{C}$ , (b) FTIR absorption spectra for  $\text{Si}_{0.984}\text{C}_{0.016}$  alloy layer after annealing at  $900^\circ\text{C}$ .



**Fig. 3.** (a) Annealing time versus integrated absorbance of FTIR at 607 cm<sup>-1</sup> for anneals at 800°C, 850°C and 900°C of the Si<sub>0.984</sub>C<sub>0.016</sub> alloy layer. (b) Activation energy for the loss of substitutional carbon obtained from FTIR. The activation energy is 2.10±0.05 eV.

in Fig. 2 for annealing at 850 or 900, the absorbance at 607 cm<sup>-1</sup> decreases while that of 810 cm<sup>-1</sup> peak increases. It is expected that carbon atoms diffuse from substitutional sites to interstitial sites, eventually forming nano-size SiC precipitates. The increased SiC precipitates in Si<sub>0.984</sub>C<sub>0.016</sub> layers are evident by the larger β-SiC phonon absorption intensity at 810 cm<sup>-1</sup>.

The relationship between absorbance due to substitutional carbon by integrated intensity and annealing time is shown in Fig. 3(a), and is fitted by exponential decay

$$a \propto \exp\left(-\frac{t}{\tau}\right) \quad (1)$$

where τ is the decay constant [17]. Figure 3(b) shows temperature dependence for decay constants representing the loss of substitutional carbon [17]. By fitting with the Arrhenius relation, the activation

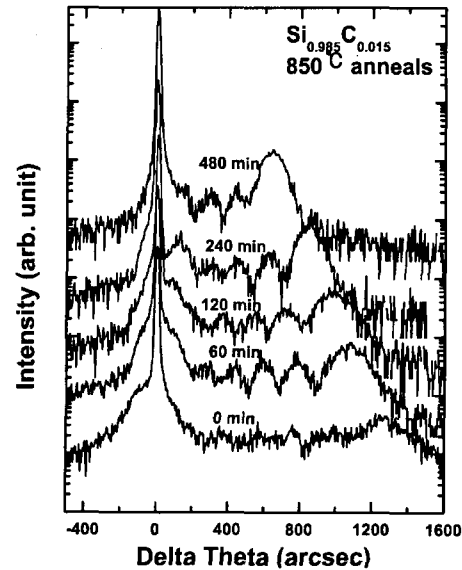


**Fig. 4.** X-ray rocking curve of the Si<sub>0.984</sub>C<sub>0.016</sub> layer after successive anneals at 850°C.

energy is obtained for the loss of substitutional carbon, 2.10±0.05 eV. Kulik *et al.* [17] reported that the activation energy  $E_a$  for the Si<sub>0.992</sub>C<sub>0.008</sub> alloy grown by molecular-beam epitaxy (MBE) was 4.45±0.15 eV. This discrepancy may be due to the difference in carbon concentration and surface oxidation during furnace annealing [19, 19]. As carbon concentration increases, carbon atoms are easy to diffuse from substitutional sites to interstitial sites during annealing. Also, the formation of SiO<sub>2</sub> may cause the injection of Si self-interstitials into Si<sub>1-x</sub>C<sub>x</sub> layer [17]. This effect with different film formation methods, SPE not MBE, may cause enhanced carbon diffusion, leading to the decreased activation energy [20-22].

In Fig. 4, x-ray rocking curves are shown for samples annealed at 850°C. The displacement of smaller satellite peak due to the epilayer is proportional to the lattice strain between Si substrate and epilayer. The substitutional carbon content is obtained from the dynamic simulation of x-ray rocking curves. Changes of the substitutional carbon concentration during annealing is shown in Figs. 5(a) and (b). Similar to the FTIR analysis, Fig. 5(c) shows the activation energy for the loss of substitutional carbon, 2.91±0.18 eV. This activation energy obtained by x-ray diffraction is in good agreement with the FTIR result (Fig. 3(b)).

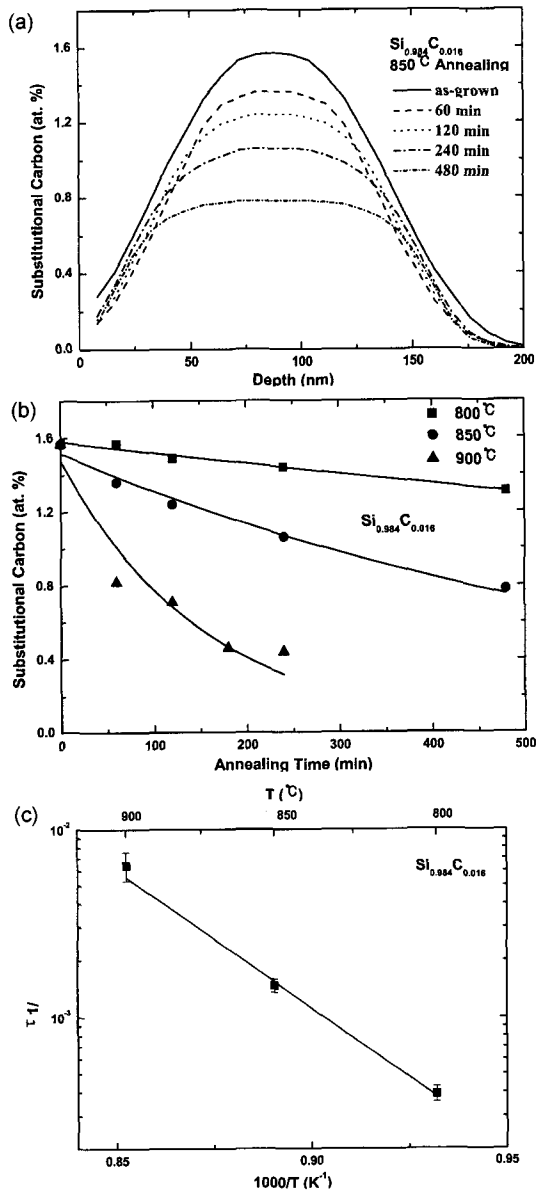


Fig. 5. (a) Substitutional carbon depth profile obtained by HR-XRD simulation (850°C annealed), (b) Annealing time versus substitutional carbon concentration for anneals at 800°C, 850°C, and 900°C. The solid lines are exponential fittings, (c) Arrhenius plot for decay constant  $1/\tau$ . The straight line is a linear fit, leading to the activation energy of  $2.916 \pm 0.18$  eV.

For the  $\text{Si}_{0.984}\text{C}_{0.016}$  layer annealed by RTA, the substitutional carbon content is similar with the layer annealed by vacuum furnace annealing, as shown in Fig. 6. These results observed in Fig. 6 show that the

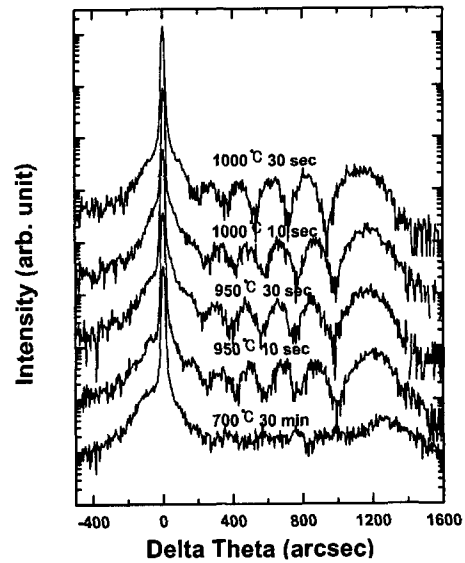


Fig. 6. X-ray rocking curve of the  $\text{Si}_{0.984}\text{C}_{0.016}$  layer annealed by RTA.

interference fringes for the layers regrown by RTA in the x-ray rocking curve is much more remarkable compared to Fig. 4. Because the interference fringe reflects the quality of the epilayer, we infer that the layers regrown by RTA have greater crystalline quality than layers regrown by vacuum-furnace annealing.

#### IV. Conclusions

We have successfully formed the  $\text{Si}_{0.984}\text{C}_{0.016}$  alloy by SPE regrowth of carbon implanted layers, and investigated the loss kinetics of substitutional carbon using FTIR and HR-XRD. The activation energy for the diffusion of substitutional carbon to interstitial sites was obtained to be  $2.10 \pm 0.05$  eV and  $2.91 \pm 0.18$  eV, respectively, from FTIR absorbance and HR-XRD. RTA looks more suitable for SPE regrowth of  $\text{Si}_{1-x}\text{C}_x$  than vacuum furnace annealing, leading to greater structural perfection for the regrowth of implanted layers.

#### Acknowledgement

The authors thank Taegon Kim (KIST, Korea) for performing ion implantation. This work is supported by the Ministry of Information & Communication of

Korea ("Support Project of University Foundation Research <1999>" supervised by IITA).

### References

- [1] H. Presting, H. Kibbel, M. Jaros, R. M. Turton, U. Menczgar, G. Abstreiter, and H. G. Grimmeiss, *Semicond. Sci. Technol.* **1**, 1127 (1992).
- [2] S. Voinigescu, M. Schumacher, K. Iniewski, R. Lisak, and Z. Parpia, *Electron Technol.* **26**, 25 (1993).
- [3] G. L. Patton, S. S. Iyer, S. L. Delage, S. Tiwari, and J. M. C. Stork, *IEEE Trans. Electron Device Lett.* **9**, 165 (1988).
- [4] S. Iyer, L. Patton, M. C. STORK, S. Meyerson, and L. Harame, *IEEE Trans. Electron Devices* **36**, 2043 (1989).
- [5] H. J. Osten, R. Barth, G. Fischer, B. Heinemann, D. Knoll, G. Lippert, H. Rucker, P. Schley, and W. Ropke, *Thin Solid Films* **321**, 11 (1998).
- [6] H. Jiang and R. G. Elliman, *IEEE Trans. Electron Devices* **43**, 97 (1996).
- [7] J. C. Sturm, *Mat. Res. Soc. Bulletin* / April 60 (1998).
- [8] S. C. Jain, H. J. Osten, B. Dietrich, and H. Rucker, *Semicond. Sci. Technol.* **10**, 1289 (1995).
- [9] P. A. Stolk, D. J. Eaglesham, H. J. Gossmann, and J. M. Poate, *Appl. Phys. Lett.* **66**, 1370 (1995).
- [10] H. J. Osten, M. Kim, G. Lippert, and P. Zaumseil, *Thin Solid Films* **294**, 93 (1997).
- [11] A. R. Powell, K. Eberl, B. A. Ek, and S. S. Iyer, *J. Crystal Growth* **127**, 425 (1993).
- [12] S. Im, J. H. Song, D. Y. C. Lie, F. Eisen, H. Atwater, and M. A. Nicolet, *J. Appl. Phys.* **81**, 1700 (1997).
- [13] J. J. Candelaria, J. K. Watanabe, N. D. Theodore, R. B. Gregory, D. K. Schroder, L. M. Stout, and N. G. Cave, *Mat. Res. Soc. Symp. Proc.* **321**, 473 (1994).
- [14] J. W. Strane, W. J. Edwards, J. W. Mayer, H. B. Stein, S. R. Lee, B. L. Doyle, and S. T. Picraux, *Mat. Res. Soc. Symp. Proc.* **280**, 609 (1993).
- [15] J. W. Strane, H. J. Stein, S. R. Lee, S. T. Picraux, J. K. Watanabe, and J. W. Mayer, *J. Appl. Phys.* **76**, 3656 (1994).
- [16] J. W. Strane, S. R. Lee, H. J. Stein, S. T. Picraux, J. K. Watanabe, and J. W. Mayer, *J. Appl. Phys.* **79**, 637 (1996).
- [17] L. V. Kulik, D. A. Hits, M. W. Dashiell, and J. Kolodzey, *Appl. Phys. Lett.* **72**, 1972 (1998).
- [18] W. K. Choi, J. H. Chen, L. K. Bera, W. Feng, and K. L. Pey, *J. Appl. Phys.* **87**, 192 (2000).
- [19] S. Zerlauth, C. Penn, H. Seyringer, G. Brunthaler, G. Bauer, and F. Schaffler, *J. Vac. Sci. Technol. B* **16**, 1679 (1998).
- [20] U. Gosele, *Mat. Res. Soc. Symp. Proc.* **59**, 419 (1986).
- [21] P. Werner, H. J. Gossmann, D. C. Jacobson, and U. Gosele, *Appl. Phys. Lett.* **73**, 2465 (1998).
- [22] R. Scholz, U. Gosele, J. Y. Huh, and T. Y. Tan, *Appl. Phys. Lett.* **72**, 200 (1998).